Plasma Induced Damage on AlGaN/GaN Heterostructure During Gate Opening for Power Devices

Running title: Plasma induced damage on AlGaN/GaN heterostructure during gate opening for power devices

Running Authors: Fesiienko Oleh

O. Fesiienko[1,2,3*], C. Petit-Etienne[1], M. Darnon[2,3], A. Soltani[2,3], H. Maher[2,3], E. Pargon[1]

[1]*Univ. Grenoble Alpes, CNRS, CEA/LETI-Minatec, Grenoble INP, LTM, F-38054 Grenoble-France*

[2]*Laboratoire Nanotechnologie Nanosystèmes (LN2) - CNRS IRL-3463, Université de Sherbrooke, 3000 Boulevard Université, Sherbrooke, Québec, Canada J1K 0A5*

[3]*Institut Interdisciplinaire d'Innovation Technologique, 3IT, Université de Sherbrooke, 3000 Boulevard Université, Sherbrooke, Québec, Canada J1K 0A5*

[*] Electronic mail: Oleh.Fesiienko@USherbrooke.ca

ABSTRACT

During the fabrication of MOS-HEMT based on AlGaN/GaN heterostructure, gate patterning is recognized as the most critical step that can lead to electrical degradation of the transistor. In this work, we performed the SiN cap layer plasma etching processes by two fluorine-based plasma processes (SF_6/Ar and CHF_3/CF_4/Ar) with low (≈15 eV) and high (≈260 eV) ion energy. Moreover, we investigate the post-etching treatment using a KOH solution in order to restore the quality of the AlGaN barrier surface after etching. The objective of this article is to evaluate the AlGaN barrier surface damage after the listed plasma etching processes and post-etching strategies by using quasi-in situ Angle-Resolved X-ray Photoelectron Spectroscopy (AR-XPS), Transmission Electron Microscopy (TEM) and atomic force microscope (AFM). Accordingly, it is found that both high ion energy plasma processes lead to a significant stoichiometric change and modification of the AlGaN barrier layer into a 1.5 nm F-rich $AlGaNF_x$ sub-surface reactive layer. The decrease

in ionic energy leads to a decrease in the SiN etch rate and a significant improvement in the SiN/AlGaN etch selectivity (which becomes infinite) for both plasma chemistries. Moreover, the decrease in ion energy decreases the depth of the modification (about 0.5 nm) and reduces the stochiometric change of the AlGaN barrier layer. However, both low and high ion energy SF_6/Ar plasma lead to 0.8 eV Fermi level shift towards the valence band. Furthermore, the KOH post-etching treatment demonstrates complete and effective removal of the $AlGaNF_x$ sub-surface reactive layer and restoration of the surface properties of the AlGaN layer. However, this removal leads to AlGaN recesses that are correlated to the thickness of the reactive layer formed during the etching.

I. INTRODUCTION

Metal Oxide Semiconductor High Electron Mobility Transistors (MOS-HEMTs) based on III-N material heterostructures such as AlGaN / GaN are recognized as excellent candidates for future generations of components for power and high-frequency electronics thanks to their two-dimensional electron gas (2DEG) with high electron density (~10^{13} cm^{-2}) and high electron mobility (~ 2000 $cm^2/V{\cdot}s$).[1,2] Typically, GaN-based HEMTs being in the ON state are also called “Normally-ON” or enhancement-mode (E-mode). For reasons of safety, energy economy, and realization of logical functions, it is necessary to make “Normally-OFF” MOS-HEMT. Different approaches exist including the implantation of fluorine ions under the gate or a gate recess process that consists of locally etching the barrier at the gate or using an ultra-thin AlGaN barrier layer.[2,3] The latter is one of the most promising integration schemes for E-mode MOS-HEMTs.[4,5] However, in the fabrication process of “Normally-OFF” MOS-HEMT using an ultra-thin AlGaN barrier layer, there are some critical technological steps that impact the performances of the HEMT transistor.

Among them, is the plasma process dedicated to the etching of the SiN cap layer necessary to open the gate region. Gate patterning by plasma etching is identified as a source of defect generation at the AlGaN/dielectric interface. Indeed, the landing on the AlGaN barrier layer can lead to severe modifications of the AlGaN barrier surface properties such as roughness, stoichiometry, surface potential modification, change of Fermi level position, as well as the formation of various other types of defects.[3,6] Therefore, the SiN etching must be stopped on the very thin AlGaN barrier layer with a nanometric control without introducing damage to the underneath AlGaN barrier layer.

In this paper, we investigate the physicochemical modifications of the AlGaN barrier surface after exposure to typical plasma etching and wet post-treatment steps used in the gate-opening process of MOS-HEMT fabrication. Several techniques such as Angle-Resolved X-ray Photoelectron Spectroscopy (AR-XPS), Atomic Force Microscope (AFM), Transmission Electron Microscopy (TEM), and in-situ kinetic ellipsometry are used to evaluate the plasma-induced damage (PID) on AlGaN surface, including stoichiometry and potential change, consumption, and roughness, as described in the experimental protocol of Section II.

In section III, we compare the impact on the thin AlGaN barrier layer of two standard Fluorine-based plasma processes (SF_6/Ar vs CHF_3/CF_4/Ar) used to etch SiN with high (≈260 eV) (section III.A.) and low (≈15 eV) ion energy (section III.B). Section III.C evaluate a wet KOH treatment to remove the damaged layer and restore the AlGaN barrier surface properties.

II. EXPERIMENTAL SETUP AND METHODOLOGY

A. Samples

In this study, two types of heterostructures are used. The first one (cf. Fig.1 (a)) is a commercial HEMT wafer (supplied by EpiGaN) grown by Metal-Organic Chemical Vapor Deposition (MOCVD) on a Si (111) substrate. The epitaxial structure consists of a 5.5 µm buffer layer, a 175 nm undoped GaN channel layer, a thin 4 nm $Al_{0.45}Ga_{0.55}N$ barrier layer, and the 50 nm-thick SiN capping layer. The structure of Fig.1 (a) is an MIS-HEMT structure that we used to evaluate the impact of the SiN opening process on the AlGaN surface by AR-XPS, AFM, and TEM analysis. However, this stack is too complex to allow the determination of SiN and AlGaN thicknesses by ellipsometry. Therefore, we used a simpler stack only for ellipsometry measurements (cf. Fig.1 (b)) that was grown by Metal-Organic Chemical Vapor Deposition (MOCVD) on a Si (111) substrate. The simpler stack consists of a 300 nm AlN thick nucleation layer, a 30 nm thick $Al_{0.45}Ga_{0.55}N$ barrier layer, and a 10 nm-thick SiN cap layer to estimate by in-situ kinetic ellipsometry the SiN and AlGaN etch rates during the plasma process. All III-N layers of Fig.1 are epitaxially grown as a polar (0001) Ga-face c-plane surface.

In the present study, all AlGaN samples (10 x 10 mm^2) are glued using a silicone-free thermal paste (type 1977-DP) from Techspray at the center of a 300 mm Si carrier wafer.

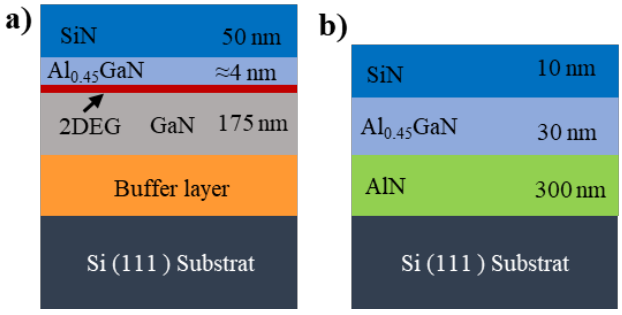

Fig. 1. Schematic of the stacks investigated in this study (a) for assessing the impact of the etching process on AlGaN and (b) for measuring SiN and AlGaN etch rates.

B. Plasma reactor

All plasma etching processes are performed in a 300 mm AdvantEdge™ MESA™ inductively coupled plasma (ICP) reactor from Applied Materials®. The plasma is created by the inductive source power via a dual radiofrequency (RF) coil and is operated at 13.56 MHz. The wafer can be RF-biased using a second power supply (capacitively coupled to the electrostatic chuck). The reactor chamber walls are coated with Y_2O_3 material. The temperatures of the reactor walls and the chuck are kept at 65 °C and 60 °C, respectively. Before each experiment, the reactor walls are cleaned by Cl_2, O_2, and NF_3-based plasma cleaning processes to obtain reproducible conditions for etching. After each process, an Ar dechuck step is used.

Fluorine-based plasmas are typically used to etch hard mask SiN.[7,8] In this article, two plasma chemistries are compared: a fluorocarbon CHF_3/CF_4/Ar chemistry and a carbon-free SF_6/Ar chemistry. The plasma parameters are given in Table I.

TABLE I. Plasma conditions used in the present work.

Process	**Parameters**					
	Gas	Flow (sccm)	Pressure (mTorr)	Source Power (W)	Bias Power (W)	
					High energy	Low energy
SiN process 1	SF_6	20	7	600	155	0
	Ar	200				
SiN process 2	CF_4	100	7	200	60	0
	CHF_3	20				

Process	Parameters					
	Gas	Flow (sccm)	Pressure (mTorr)	Source Power (W)	Bias Power (W)	
					High energy	Low energy
	Ar	200				

These two plasma conditions are standard processes that we are using in our tool to open SiN with anisotropic profiles. Fig.2 compares the ion velocity distribution function (IVDF) of these two processes obtained with a retarding field energy analyzer (RFEA). A complete description of the RFEA that is used in this work can be found elsewhere.[9] Both plasma conditions show a bimodal distribution due to the sheath potential oscillation. The mean ion energy in the high-energy SF_6/Ar plasma is lower (157 eV) than in the high-energy CHF_3/CF_4/Ar plasma (200 eV), but the ion energy distribution is wider resulting in ions with similar energy in the highest range (155-160 eV). The maximal ion energy is similar for both plasma processes (about 260 eV). Moreover, the peak area that is proportionally related to the ion flux is 3.8 times higher in the case of the SF_6/Ar plasma. To estimate the ion flux, measurements are performed using a capacitive planar probe[10] installed on the wall of the reactor chamber. We measured an ion flux of 0.165 mA/cm^2 and 0.637 mA/cm^2 for CHF_3/CF_4/Ar and SF_6/Ar plasma, respectively. This low ion flux indicates a low ion plasma density in both cases ($<10^{11}$ cm^{-3}).

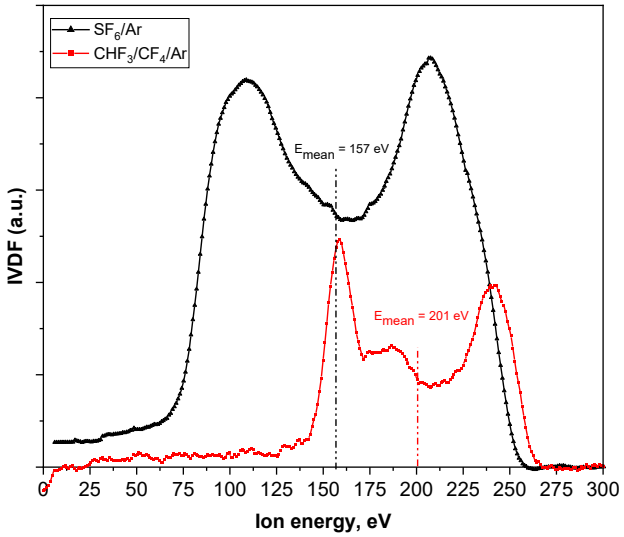

Fig. 2. Measured average ion velocity distribution function (IVDF) during high-energy SF_6/Ar plasma (black line) and high-energy CHF_3/CF_4/Ar (red line) plasma etching processes.

Regarding the plasma composition, optical emission spectroscopy (OES) was performed with an end-point system, EyeD ™ from Verity Instrument. OES demonstrates the presence of F species but also the presence of SiF_x species that result from the etching of the Si carrier wafer for high-energy SF_6/Ar plasma (cf. Fig.3 (a)). In the case of the high-energy CHF_3/CF_4/Ar plasma, we observe the presence of CF_x, Ar, and F radicals (cf. Fig.3 (b)). According to K. Takahashi and X. Huang the CF_x, Ar, F, and H radicals are the main products of the decomposition of CHF_3/CF_4/Ar.[11,12] However, in the case of high-energy CHF_3/CF_4/Ar plasma, it's not observed the presence of the H radicals by OES which may be explained by the recombination of F and H radicals.

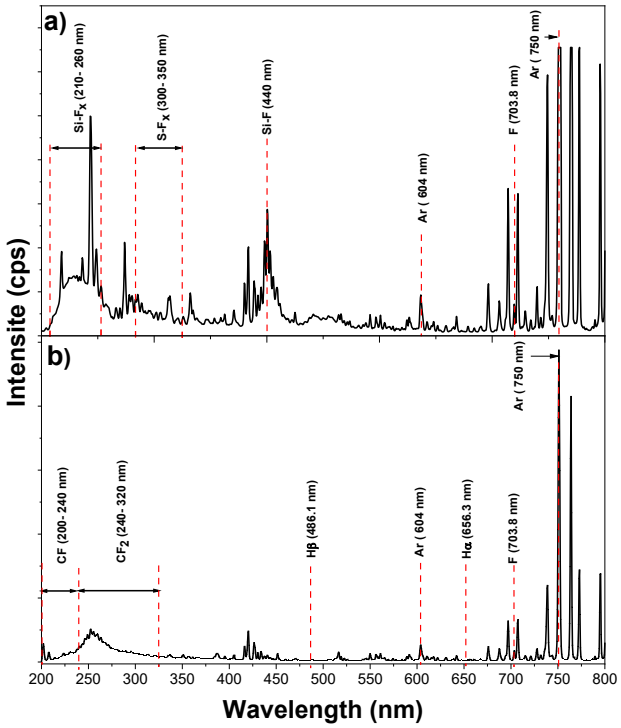

Fig. 3. Optical emission spectra recorded during SiN plasma etching (a) by high-energy SF_6/Ar plasma and (b) by high-energy CHF_3/CF_4/Ar plasma.

To evaluate the Etch rates of SiN and AlGaN exposed to fluorine-based plasma processes, in-situ ellipsometry measurements using an UVISEL ellipsometer from Jobin Yvon connected to the reactor are performed on the samples of Fig1.(b). The spectroscopic acquisitions are done in the 1.5-5 eV range with a step size of 0.05 eV at an analysis angle of 60°. The thicknesses of the material are obtained thanks to the DeltaPsi II software, developed by Horiba/Jobin Yvon.

The ellipsometric model uses a SiN/AlGaN/AlN/Si bulk stack. The dispersion laws used for SiN, AlGaN, and AlN are New amorphous (derived on the basis of Forouhi-Bloomer formulation), Tauc Lorentz, and Classical dispersion models proposed by Delta-Psi software, respectively. [13] Three ellipsometry measurements are needed to estimate the etch rate of SiN and AlGaN. The first one is performed before etching allowing the

determination of initial SiN, and AlGaN thicknesses. The SiN is then etched and the etching step is stopped at the endpoint detection. This allows us to estimate the SiN etch rate. The second measurement is done at this stage to get the AlGaN thickness before etching. Then this AlGaN layer is exposed to a 60s plasma process and a third ellipsometry measurement is done for AlGaN etch rate determination.

C. Angle-Resolved X-ray Photoelectron Spectroscopy AR-XPS

The chemical composition of the AlGaN surface after SiN etching is examined with quasi-in situ Angle-Resolved X-Ray Photoelectron Spectroscopy (AR-XPS, Thermo Fisher Theta 300). The XPS analysis chamber is connected to the reactor via a vacuum transfer chamber, allowing quasi-in situ surface characterization. X-ray photons are generated with a monochromatic Al Kα X-ray source (1486.6 eV). The pass energy and dwell time are set at 60 eV and 500 ms, respectively for standard and angle-resolved XPS. A combined Thermo Fisher Scientific dual Ar ion and electron flood gun is used in order to compensate for the surface charging effects with minimal surface damage.[14] A more detailed description of this technique is given elsewhere.[14]

The angular mode uses eight angles regularly spaced between 23.75° and 76.25°, referred to as the normal of the wafer (*i.e.* collection angle). The angles of 23.75° and 76.25° correspond to photoelectrons escaping from the bulk (about 8 nm) and near-surface (about 2 nm), respectively.[15]

As the AlGaN layer thickness is about 4 nm, we estimate from IMPF calculations that the angle of 53.25° is the most appropriate to probe the whole AlGaN layer with the minimal signal from underneath GaN.[15] In order to investigate the reactive layer

composition formed after plasma exposure, and surface properties change, the angle of 76.25° is used and the values are compared to the reference ones at 53.25°.

A genetic algorithm based on the maximum entropy method (provided by Thermo Fisher Scientific) is used to reconstruct atomic composition depth profiles from angle-resolved AR-XPS data.[16] In this study, we have used the Ga*3d*, Al*2p*, N*1s*, O*1s*, C*1s*, F*1s*, S*2s*, and Si*2s* core-level energy regions to extract the concentration of Ga, Al, N, O, C, F, S, and Si atoms, respectively. The peaks are decomposed and fitted using a numerical fitting procedure in the Advantage^{TM} software. The background subtraction is performed by using a Shirley function. Element concentration is obtained by using the corresponding Al Scofield cross-section peak.[17] The concentration of each element is obtained by dividing each peak area by the corresponding Scofield cross-section (Ga*3d*: 1.085, Al*2p*: 0.537, N*1s*: 1.8, O*1s*: 2.93, C*1s*: 1.0, F*1s*: 4.43, S*2s*: 1.43, Si*2s*: 0.95). A more detailed description of the technique is given elsewhere.[18] All XPS spectra are calibrated in energy by positioning the Al*2p* peak corresponding to the Al-N bonds at 74.0 eV.

To obtain the XPS reference spectrum of the AlGaN surface, the sample in Fig.1 (a) is immersed in a BOE bath for 24 hours in order to completely remove the SiN with minimal damage to the surface of the AlGaN. Fig.4 shows the decomposition of the XPS peaks for the (a) Ga*3d*, (b) Al*2p*, and (c) N*1s* spectra of the reference AlGaN surface.

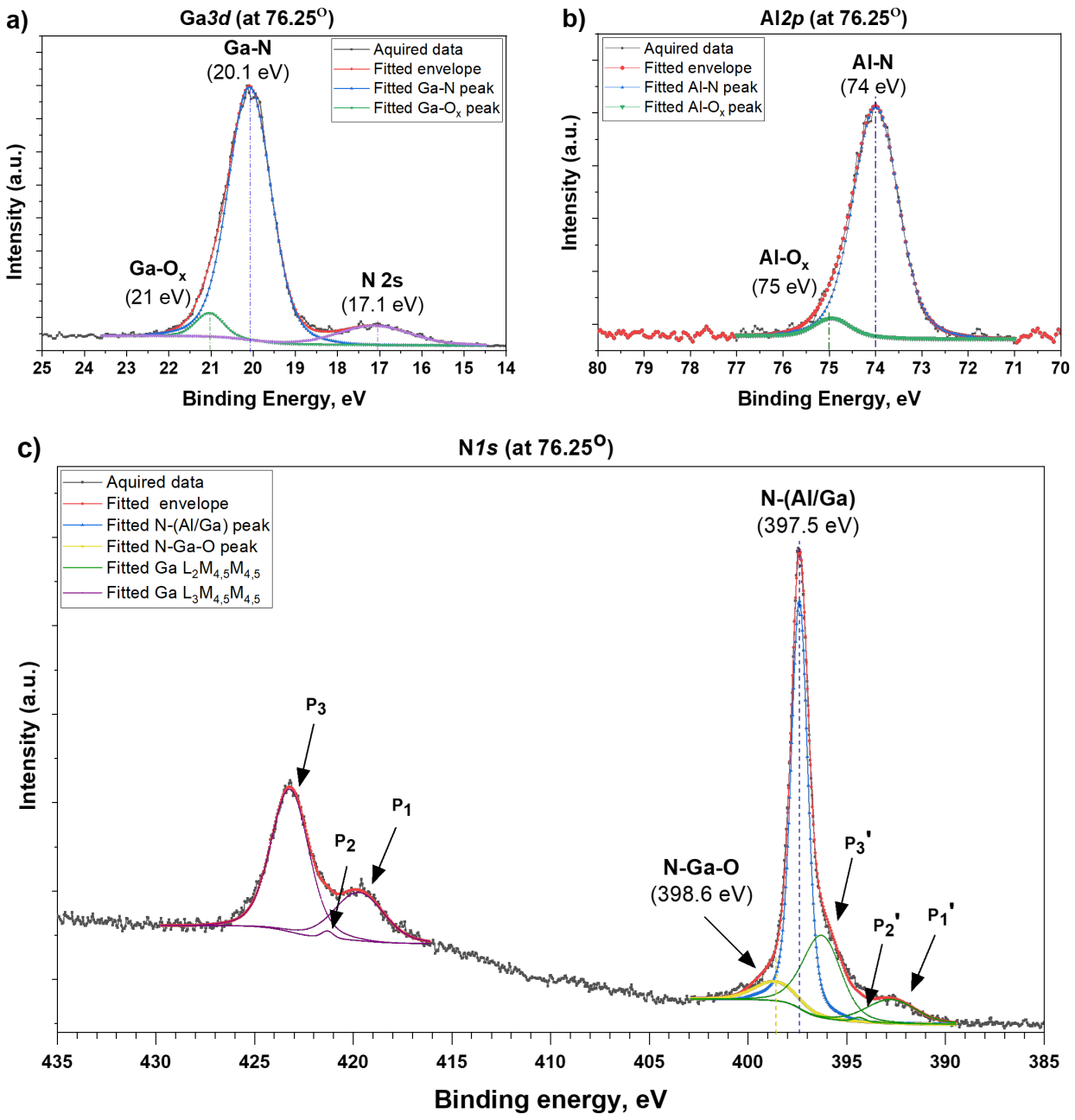

Fig. 4. (a) Ga*3d*, (b) Al*2p*, and (c) N*1s* core levels deconvolution of AR-XPS spectra of the reference AlGaN sample measured at 76.*25*°.

As shown in Fig.4 (a), the Ga*3d* is fitted with three peaks at 17.1 eV, 20.1 eV, and 21.0 eV corresponding to an overlapped N*2s* core level, Ga-N, and Ga-O_x (native oxide) bonds, respectively. The Al*2p* is fitted with two peaks at 74.0 eV and 75.0 eV attributed to

Al-N and Al-O_x (native oxide) bonds, respectively. The N*1s* peak overlaps with the LMM Auger lines of Ga. To decompose properly the N*1s* spectrum and eliminate the Auger contribution, we have used the methodology proposed by Meyer *et al.*[15] This fitting procedure allows decomposing of the N*1s* spectrum with two contributions located at 397.4 eV and 398.6 eV. These contributions correspond to N-(Al/Ga) bonds and N-Ga-O bonds, respectively. Table II summarizes the XPS results obtained on the AlGaN reference in terms of detected chemical elements on the surface and their chemical environment and their relative atomic concentration for the surface and bulk of the AlGaN layer.

TABLE II. The element and corresponding core level, the chemical bond and corresponding binding energies (BE), full width at half maximum (FWHM), and atomic percentage of the reference AlGaN layer measured by AR-XPS at bulk (53.25°) and surface (76.25°) grazing angle.

Element	Core level	Chemical bond	BE, eV	FWHM, eV	Atomic %	
					Bulk	Surface
Ga	*3d*	Ga-N	20.1 ± 0.1	1.2	24	14
		Ga-O_x	21.0 ± 0.1	0.8	0	>1
Al	*2s*	Al-N	74.0 ± 0.1	1.2	22	16
		Al-O_x	74.9 ± 0.1	0.9	0	>1
N	*1s*	N- (Al/Ga)	397.4 ± 0.1	1.0	37	23
		N-Ga-O	398.6 ± 0.1	2.5	1	4
C	*1s*	C-C	284.7 ± 0.1	1.6	5	14
		C-O	286.1 ± 0.1	2.3	>1	3
		C=O	289.3 ± 0.1	2.4	0	2
O	*1s*	O_X-(Al/Ga)-N	531.2 ± 0.1	1.8	5	6
		OH^-	532.6 ± 0.1	1.9	2	7
Si	*2s*	Si-(N/Al/Ga)	153.2 ± 0.1	3.0	>1	3
F	*1s*	Not attributed	684.9 ± 0.1	1.5	3	4
		Not attributed	686.6 ± 0.1	2.1	>1	2

The O*1s* peak is decomposed into two components at 531.3 eV assigned to the O_x-(Ga/Al)-N chemical bonds and at 532.5 eV attributed to O_x-C bounds. The presence of these chemical bonds is due to the natural Al and Ga oxidation and the C-O_x adsorption on the AlGaN surface in the air. After the BOE treatment, F, Si, and C contamination are also detected. The Si*2s* spectra present one peak at 153.2 eV (+2.2 eV chemical shift compared

to Si-Si bonds). We think that it corresponds to Si-N-(Al or Ga) bonds grafted to the AlGaN surface that cannot be removed by the BOE. The C*1s* spectra are fitted with three peaks that are located at 284.6 eV (C-C bonds), 286.0 eV (C-O bounds), and 289.2 eV (C=O bounds). The presence of carbon peaks is due to air exposure. The F*1s* core level indicated F contamination. This contamination is not attributed to chemical bonds and is due to residual contamination from the BOE bath and from the transfer from the plasma reactor to the XPS chamber. All fitted peak positions are in agreement with values in the scientific literature.[19,20]

The reference stoichiometry of our AlGaN film is estimated by calculating the Ga/Al and (Al+Ga)/N ratios obtained from the XPS spectra of the AlGaN sample after BOE collected at a 53.25° angle. The Ga/Al and (Al+Ga)/N ratios take into consideration all Ga*3d* (Ga-N + Ga-O_x), Al*2p* (Al-N + Al-O_x), and N*1s* (N-(Ga/Al) + N-Ga-O) contributions. Thus, the reference ratios of the AlGaN films are 1.1 for Ga/Al and 1.2 for (Al+Ga)/N. To evaluate the AlGaN surface stoichiometry change after plasma exposure, the ratios are calculated from the XPS spectra collected at 76.25° and compared to the reference ratios.

The XPS spectrum in the energy region of 0-15 eV corresponds to the AlGaN valence band spectrum. This spectrum can be used to evaluate the valence-band maximum energy (E_{VBM}) of the AlGaN layer.[21] The valence band maxima (E_{VBM}) is determined by extrapolating a linear fit of the leading edge of the valence band photoemission to the baseline, as shown in Fig.5. Assuming the 0 eV position as the Fermi level (E_F), we can estimate Fermi level evolution of the AlGaN barrier layer, which reveal the (sub-)surface modification.[21] For the reference sample (after BOE), the E_F-E_{VBM} is 2.5 eV.

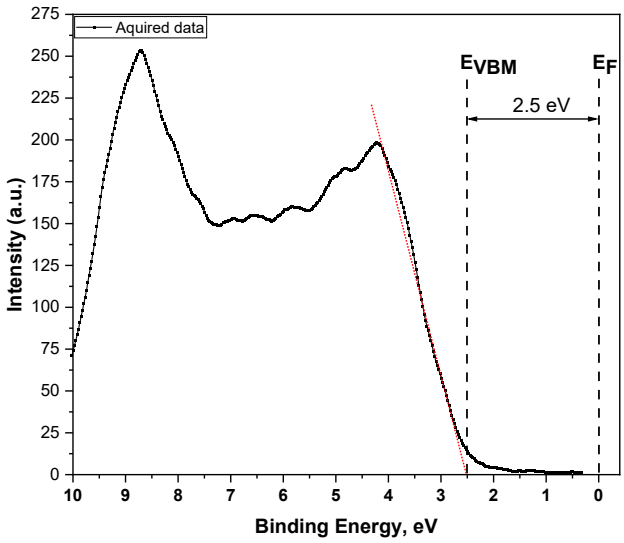

Fig. 5. Valence-band spectrum for the reference AlGaN sample.

D. Transmission Electronic microscopy (TEM)

Transmission Electron Microscopy (TEM) is performed in order to observe the thickness of the AlGaN layer consumed during the SiN etching step. The observations are performed in a TEM TECNAI with an incident beam energy of 200 keV. A dual-focused ion beam scanning electron microscope (FIB-TEM) provided by FEI Helios 450S is used to prepare the 100 nm thick lamella for the TEM characterizations.

E. Atomic force microscopy (AFM)

Atomic force microscopy (AFM) is used to measure the surface roughness of the AlGaN samples after different etching and post-etching treatments. In our study, we use Atomic Force Microscope (AFM) FastScan from Bruker. The measurements were performed in a ScanAssist mode. To perform the analysis, we used a silicon tip on a silicon nitride cantilever, type FASTSCAN-A from Bruker. The scanning area was set as 5×5 μm^2, 1×1 μm^2, with 16.22 nN applied force and the scanning rate was 2 Hz for a resolution of 512 × 512 data points.

III. RESULTS AND DISCUSSION

A. Preliminary studies of conventional plasma process for SiN etching

Samples of Fig.1 (b) are exposed to the SiN opening processes described in Table I. The etch rates of the SiN and AlGaN layers during the fluorine-based processes are estimated by in situ spectroscopic ellipsometry to 1.5 nm/s and 0.4 nm/s for the high energy SF_6/Ar plasma and 0.8 nm/s and 0.1 nm/s for the high-energy CHF_3/CF_4/Ar plasma, respectively. The results obtained in terms of etch rates and SiN/AlGaN etch selectivity for the two investigated processes are summarized in Table III.

TABLE III. The etch rates of SiN and AlGaN measured by ellipsometry during the high-energy and low-energy SF_6/Ar and CHF_3/CF_4/Ar plasma etching processes.

Plasma chemistry	Etch rate SiN (nm/s)	Etch rate AlGaN (nm/s)	SiN/AlGaN etch selectivity
High-energy SF_6/Ar	1.5	0.4	4
High-energy CHF_3/CF_4/Ar	0.8	0.1	6
Low-energy SF_6/Ar	0.2	0	∞
Low-energy CHF_3/CF_4/Ar	0.1	0	∞

For a similar maximum ion energy, the high-energy SF_6/Ar plasma process leads to 1.9 times higher etch rates SiN and 4 times higher AlGaN etch rates than the high-energy CHF_3/CF_4/Ar plasma process. Consequently, the SiN/AlGaN selectivity is 1.5 times higher in the case of high-energy CHF_3/CF_4/Ar compared to the high-energy SF_6/Ar process (cf. Table III). The higher ion flux for the high-energy SF_6/Ar plasma can explain this effect. Indeed, the ion flux for the high-energy SF_6/Ar plasma (0.637 mA/cm^2) is three times more important than for the high-energy CHF_3/CF_4/Ar plasma process (0.165 mA/cm^2). Based on the etch rates estimated with samples of Fig.1 (b) and thanks to the endpoint detection

(EyeD^{TM}) system, the samples of Fig.1 (a) are etched using the fluorine-based plasma and the SiN process is stopped on the AlGaN surface without applying over-etching time (less than 5s of over-etch). The chemical composition of the AlGaN surface exposed to the two high-energy SiN etching processes is characterized by quasi-in-situ AR-XPS analyses.

Fig.6 (a) shows the XPS analysis of the surface composition (at grazing angle 76.25°) of AlGaN after SiN etching by high-energy SF_6- and CHF_3-based plasma processes. In both cases, a significant amount of fluorine of about 40% (with two F*1s* peaks located at 685.2 and 686.9 eV) is detected on the surface (cf. Fig.6 (a)). Moreover, the XPS spectra of Ga*3d*, Al*2p*, and N*1s* core levels show the appearance of new chemical environments (cf. Fig. 6 (b), (c), and (d)).

For the Ga*3d* core level in Fig.6 (b), three new components are found at 21.0 eV, 21.8 eV, and 22.5 eV after high-energy CHF_3/CF_4/Ar plasma and one new component at 21.1 eV after high-energy SF_6/Ar plasma etching. The peaks at 21.0, 21.8, and 22.5 eV are attributed to Ga-F, Ga-F_2, and Ga-F_3 compounds.[22,23] For the Al*2p* core level in Fig.6 (b), two new peaks at 75.8 and 76.7 eV are detected and attributed to Al-F_x and Al-F_3 bonds as reported by several.[24] The Al-F_x and Al-F_3 peaks are present for both plasma chemistries and constitute about 8% of the total atomic quantification.

The N*1s* core level shows two contributions positioned at 397.5 and 399.2 eV for both plasma processes, attributed to N-(Ga/Al) and N-F_x bonds respectively. In addition, the different peaks located at P_1' at 392.7 eV, P_2' at 394.3 eV, and P_3' at 396.2 eV in the N*1s* spectrum region (cf. Fig. 6 (d)) are assigned to the auger peaks of Ga ($L_2M_{4,5}M_{4,5}$). In the high-energy CHF_3/CF_4/Ar case, we observe two new contributions at 398.4 eV labeled P_4' and at 400.5 eV labeled P_5'. These contributions can be attributed to the Ga auger ($L_2M_{4,5}$

$M_{4,5}$) peaks of Ga-F_2 and Ga-F_3 bonds respectively. Meanwhile, no auger peak for Ga-F is observed. This can be explained by the superposition of the auger peaks Ga-F and Ga-N (confirmed by the augmentation of FWHM of the P_3' peak from 2.3 eV up to 2.5 eV). On the other hand, when high-energy SF_6/Ar plasma is used, the appearance of a new P_4' and P_5' due to the formation of Ga-F_x bonds is not visible. This can be explained by the absence of the high-level fluorinated Ga-F_2 and Ga-F_3 compounds (cf. Fig.6 (b)).

In the case of high-energy CHF_3/CF_4/Ar plasma, C*1s* and O*1s* are also detected. The C*1s* spectrum shows 4 components at 285.2 eV, 286.8 eV, 288.1 eV, and 289.0 eV that are respectively attributed to C-C (14 %), C-C-F (5 %), C-F (4 %), C-F_2 (3 %) bonds.[25] This confirms the formation of a carbon-rich fluorocarbon reactive layer on the AlGaN surface. The O*1s* core level shows one contribution positioned at 532.8 eV (about 9 %) and attributed to loosely bonded oxygen at the surface.[26] The detected oxygen is suspected to be the contamination from the Y_2O_3 reactor wall sputtered by the plasma ions. In the case of high-energy SF_6/Ar plasma, the C (about 4 %) and O (about 11 %) are also detected and are supposed to come from reactor wall contamination. Moreover, a Si peak is detected at 154.0 eV that we attribute to Si-F_x or Si-O-F_x bonds. OES presented in Fig.3 shows the presence of SiF_x species in the plasma coming from the etching of the Si substrate in high-energy SF_6/Ar plasma. It is suspected that those SiF_x species participate in the AlGaN etching. Indeed, the Si carrier wafer is etched more significantly during the high-energy SF_6/Ar process (3.4 nm/s) than with the high-energy CHF_3/CF_4/Ar process (0.6 nm/s).

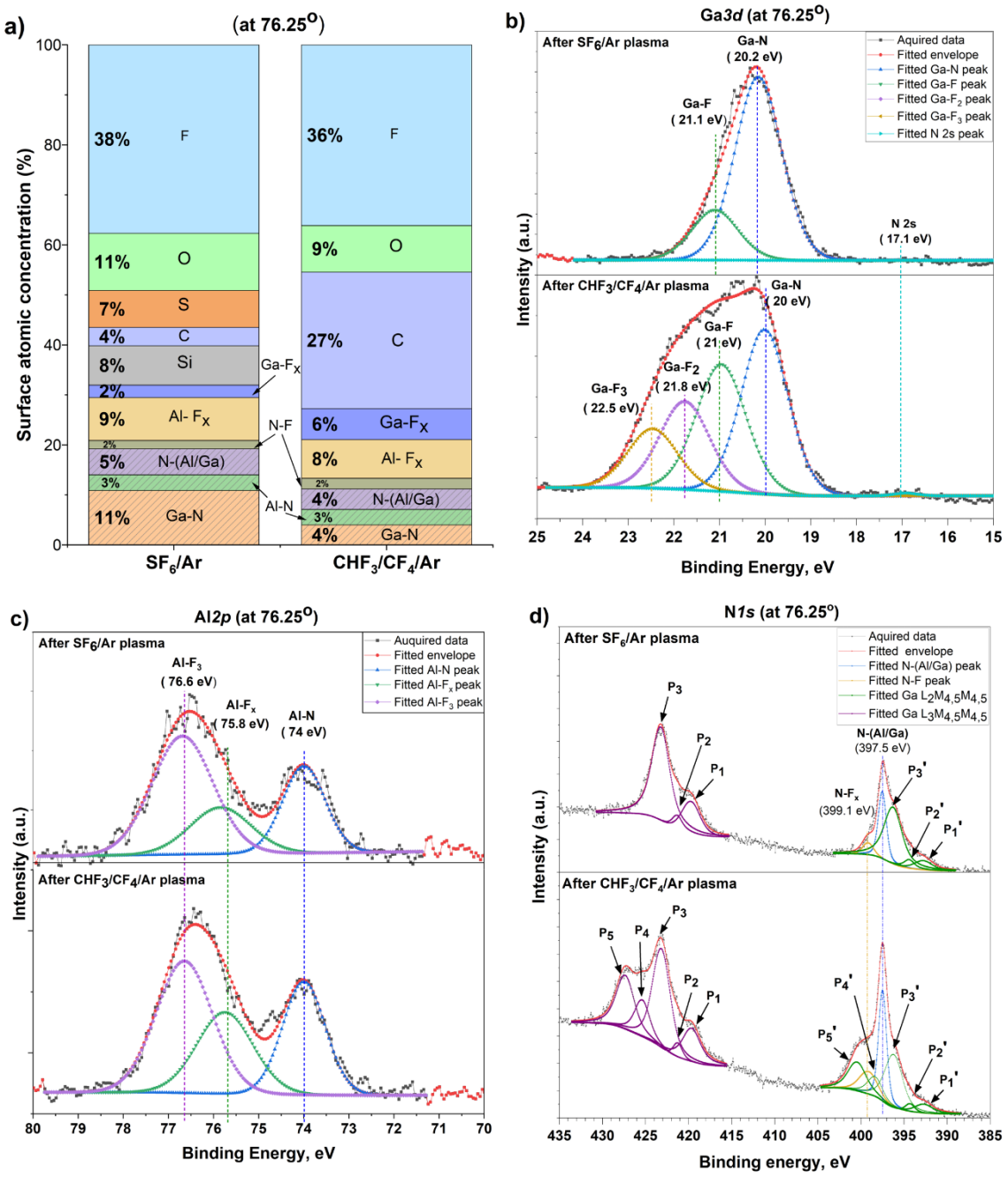

Fig. 6. (a) Surface atomic concentration and (b) Ga*3d*, (c) Al*2p*, and (d) N*1s* core levels spectra of the AlGaN surface after SiN etching by high-energy SF_6/Ar and high-energy CHF_3/CF_4/Ar plasma processes measured by AR-XPS at a grazing angle of 76.25°.

Thanks to the angle-resolved capability of AR-XPS, the in-depth profiles (cf. Fig.7 (a) and (b)) of the atomic element concentrations of the AlGaN surface exposed to both

plasma chemistries can be obtained. In this graph, the AlGaN concentration includes the contributions of the Al-N, Ga-N, and N-(Ga/Al) peaks identified to come from the non-modified AlGaN layer, while the reactive layer consists of Al, Ga, and N in another chemical environment as well as contaminants. These contaminants can be classified into two categories:

1) The elements forming bonds with the initial AlGaN matrix, *i.e* F in the high energy $CHF_3/CF_4/Ar$ and SF_6/Ar case (F-based contamination in Fig.7 refers to all Al-F_x, Ga-F_x, N-F_x, and F peaks);
2) The other detected elements that do not form bonds with AlGaN (C, O, Si, and S).

In both cases, most contaminants are in the first 1 nm at the surface, while fluorine is observed deeper in an F-rich $AlGaNF_x$ layer. The thickness of the reactive layer is slightly higher for the $CHF_3/CF_4/Ar$ process (1.5 nm for SF_6/Ar and 1.7 nm for $CHF_3/CF_4/Ar$). The damage depth is mainly related to the ion energy which is slightly higher in $CHF_3/CF_4/Ar$ (cf. Fig.2). The presence of a fluorine-rich $AlGaNF_x$ reactive layer when AlGaN is exposed to fluorine-based plasma is explained by the high reactivity of F with Ga and Al to form very stable and low volatile Al-F_x and Ga-F_x compounds (Al-F_3 boiling point at atmospheric pressure 1272 °C, Ga-F_3 boiling point at atmospheric pressure 1000 °C).[27] This low volatile $AlGaNF_x$ layer formation explains why the etch rates of AlGaN in fluorine-based plasmas are so low compared to SiN with which volatile Si-F_x (boiling point at atmospheric pressure -86 °C) and N-F_3 (boiling point at atmospheric pressure -128 °C) products can be formed.[27] Therefore, a high SiN/AlGaN etch selectivity can be obtained in fluorine-based plasma.

The etching of the AlGaN in fluorine-based plasma proceeds through the sputtering of the $AlGaNF_x$ layer. The sputtering rate depends linearly on the ion flux and the square root of the ion energy.[28] Therefore, even if the mean ion energy in the high-energy SF_6/Ar plasma is slightly lower than in the high-energy CHF_3/CF_4/Ar plasma, the three-fold larger ion flux in SF_6/Ar plasma compared to CHF_3/CF_4/Ar plasma leads to an etching rate about three times higher.

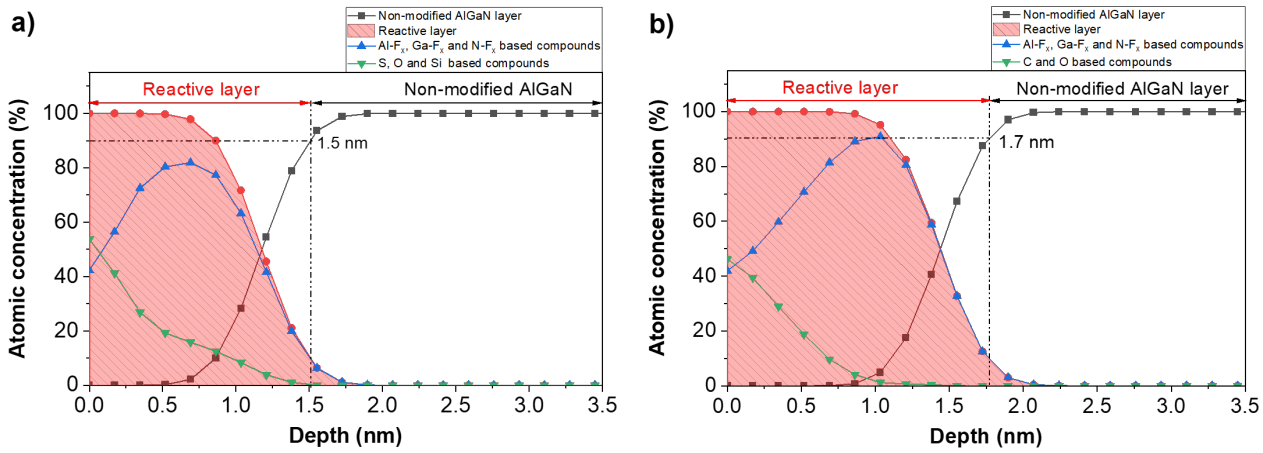

Fig. 7. Atomic concentration profiles measured by AR-XPS after SiN layer etching by (a) high-energy SF_6/Ar plasma, and (b) high-energy CHF_3/CF_4/Ar plasma.

The AlGaN surface stoichiometry ratios for reference AlGaN sample and after exposure to fluorine-based plasmas are compared in Fig.8. Both plasma processes lead to N depletion, but it is more pronounced with the high-energy SF_6/Ar plasma process. This is not surprising, given that nitrogen can form more volatile products with fluorine such as $N\text{-}F_3$, which boiling point at atmospheric pressure is -129 °C, while metal elements such as Al and Ga form the more stable compounds such as $Al\text{-}F_3$, and $Ga\text{-}F_3$.[27] Moreover, N being lighter can be more easily sputtered than Ga or Al.

Moreover, the Ga/Al ratio after high-energy CHF_3/CF_4/Ar plasma exposure is decreased indicating a slightly preferential removal of Ga compared to Al (cf. Fig.8) while the ratio Ga/Al seems non-impacted in high-energy SF_6/Ar plasma. This can be explained by the presence of HF^+ in the high-energy CHF_3/CF_4/Ar plasma as confirmed by several scientific works.[11] Those H-based ions can contribute to Ga removal by the formation of volatile Ga-H_3 (boiling point at atmospheric pressure 0 °C) compounds explaining why the AlGaN surface is more depleted in Ga with high-energy CHF_3/CF_4/Ar plasma.

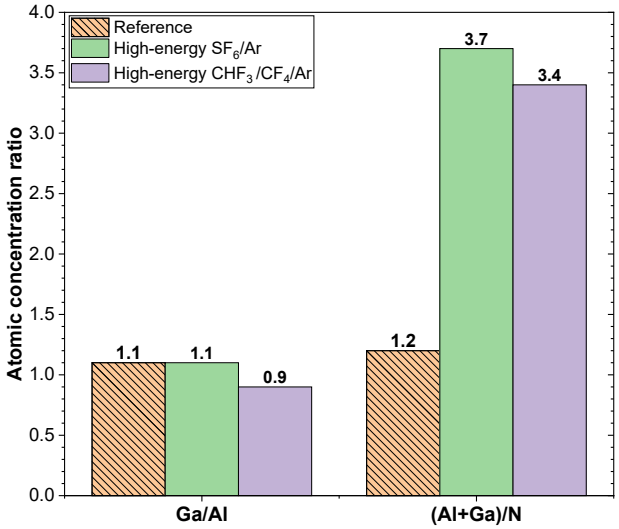

Fig. 8. The Al/Ga and (Al+Ga)/N ratios according to the plasma chemistry.

In addition, the E_F-E_{VBM} determined for both high-energy processes is compared to the reference values in Table IV.

TABLE IV. The E_F-E_{VBM} of the AlGaN surface for the reference sample and the samples after high-energy SF_6/Ar and high-energy CHF_3/CF_4/Ar plasma etching processes, extracted from the valence-band XPS spectrum.

Samples	E_F-E_{VBM} (eV)
Reference	2.5
High-energy SF_6/Ar	1.7
High-energy CHF_3/CF_4/Ar	2.3

The E_F-E_{VBM} after plasma exposure is reduced in both cases but the decrease is more pronounced with the high-energy SF_6/Ar plasma (about 0.8 eV). This change is due to the formation of the F-rich $AlGaNF_x$ layer by fluorine-based plasma exposure. A possible cause of this change is plasma-induced damage, such as the elimination of donor surface states like the N-vacancy (V_N) or the creation of acceptor surface states like the Ga or Al-vacancy (V_{metal}), or the implantation of F.[29] In the case of high-energy SF_6/Ar plasma, the significant N depletion and high flow of F^+/F lead to the formation of the surface complex. This complex behaves as donor-like states and leads to the 0.8 eV Fermi level shift closer to the valence band. Therefore, various kinds of operation instabilities in AlGaN/GaN HEMTs can be created as reported in several papers.[3,29]

To summarize this part, we have seen that the etching of the AlGaN barrier layer in high-energy fluorine plasma proceeds through the sputtering of a low-volatile $AlGaNF_x$ reactive layer. The processes having similar maximum ion energy, the thickness of the $AlGaNF_x$ layer is equivalent in both plasma conditions and around 1.5 nm. The sputtering of this layer is mostly driven by the ion flux and is three times larger for SF_6/Ar plasma compared to CHF_3/CF_4/Ar plasma. Both plasma chemistries lead to a significant surface modification such as nitrogen depletion, and modification of the first 1.5-1.7 nm of the AlGaN barrier layer into Al-F_x and Ga-F_x-based compounds. This plasma treatment of the AlGaN surface leads to the modification of the surface electronic states in the first atomic layers, as well as the modification of the piezoelectric and spontaneous polarizations of the AlGaN barrier layer influencing the density of electrons in 2DEG.[30] The Fermi level (E_F-E_{VBM}) changes in both plasma strategies used but the impact is more important with high-energy SF_6/Ar plasma. This modification can change into static negative charges by

capturing electrons. Therefore, the creation of negative charges in the AlGaN barrier layer occurs. All listed modifications can induce the degradation of the electrical properties and can directly influence the behavior of the 2DEG channel (degrading the density) due to the specificity of our integration with a thin AlGaN barrier layer.[3] We can therefore conclude that plasma etching processes lead to a significant surface modification that can be directly linked to the ion energy. We will therefore investigate in the next part the impact of lower ion energy processes on the AlGaN barrier surface.

B. Low-energy fluorine-based plasma process

This section presents the study of the impact of plasma ion energy on the surface of the AlGaN barrier exposed to the SiN plasma etching process. In order to limit the degradation of the AlGaN barrier layer, the SF_6/Ar and CHF_3/CF_4/Ar plasma processes with low-energy (0W bias power) are studied. Samples of Fig.1 (b) are exposed to the low-energy SiN opening processes described in Table I. The RFEA measurements indicate that ions have an energy of about 15 eV for both plasma processes. Table III shows the etch rate and selectivity for all processes. With the low-energy processes, an etch rate of 0.2 nm/s and 0.1 nm/s is measured for SiN in SF_6/Ar and CHF_3/CF_4/Ar plasmas, respectively, while no etching can be measured for AlGaN, indicating an infinite selectivity in both cases (cf. Table III). Those low ion energy processes show too low SiN etch rates to be used to etch the 50 nm thick SiN layer. However, they can be used as a soft-landing and over-etch step to etch the last 5 nm of SiN and land softly on the AlGaN layer.

AR-XPS experiments are performed after plasma exposure of the samples presented in Fig.1 (a) for both low-energy plasma conditions. The decomposition of the XPS peaks is identical to the one described in section III.A. for the samples etched by high-

energy SF_6/Ar and CHF_3/CF_4/Ar plasma, respectively. From the XPS peaks deconvolution, the atomic chemical composition of the AlGaN surface exposed to low-energy SF_6/Ar and CHF_3/CF_4/Ar plasma is extracted. Both low-energy plasma processes lead to a modification of the AlGaN surface similar to the one observed in the high-energy plasma (cf. Fig.6). It is observed that a fluorine-rich $AlGaNF_x$ reactive layer is formed (with the formation of Al-F_x and Ga-F_x bonds) combined with CF_x contaminants in the case of CHF_3/CF_4/Ar plasma chemistry and with Si, S contaminants for SF_6/Ar.

Fig.9 demonstrates the ratio Al-F_x/Ga-F_x present in the reactive layer for both plasma chemistry and two ion energies. For all tested conditions, the reactive layer is richer in Al-F_x bonds than Ga-F_x. In particular, for the SF_6/Ar plasma chemistry, there are three times more Al-F_x than Ga-F_x. The fluorination of Al is favored over the one of Ga. However, the energy of the ions does not affect the ratio significantly.

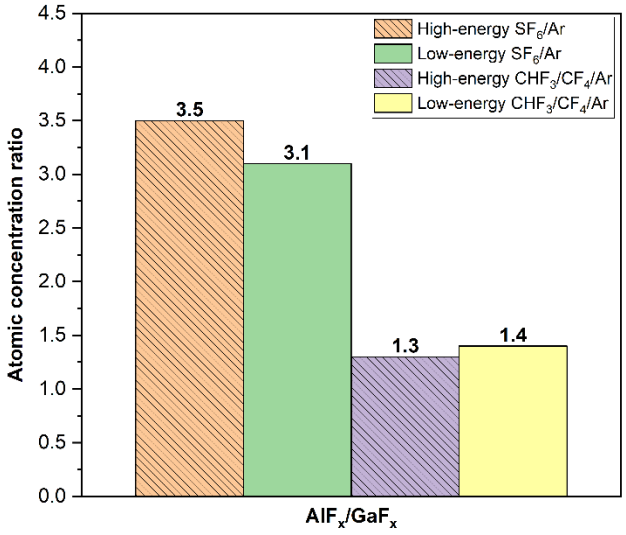

Fig. 9. The Al-F_x/Ga-F_x ratio of the AlGaN surface after low-energy SF_6/Ar and low-energy CHF_3/CF_4/Ar plasma etching extracted from the AR-XPS spectra measurements at surface grazing angle 76.25°.

The in-depth atomic concentration profiles extracted from the AR-XPS data presented in Fig.10 (a) and (b) give an insight into the thickness of the surface-modified layers. In both cases, the modified layer is about 1 nm, thinner than the layer formed by high ion energy processes (1.5 nm). A thicker reactive layer with higher ion energy is not surprising and is consistent with other experimental or modeling works[31] The Stopping and Range of Ions in Matters (SRIM) Monte Carlo simulations developed by Ziegler[32] predict that an Ar ion at 15 eV and 260 eV can penetrate into AlGaN as deep as 0.5 nm and 1.3 nm respectively. It can be noticed that the thicknesses of the fluorinated layers obtained by AR-XPS measurements are greater than the values estimated by the SRIM simulation, especially at low-energy processes. This could indicate that fluorine is able to diffuse deeper than the penetration depth of the ions to form Al-F_x and Ga-F_x bonds.

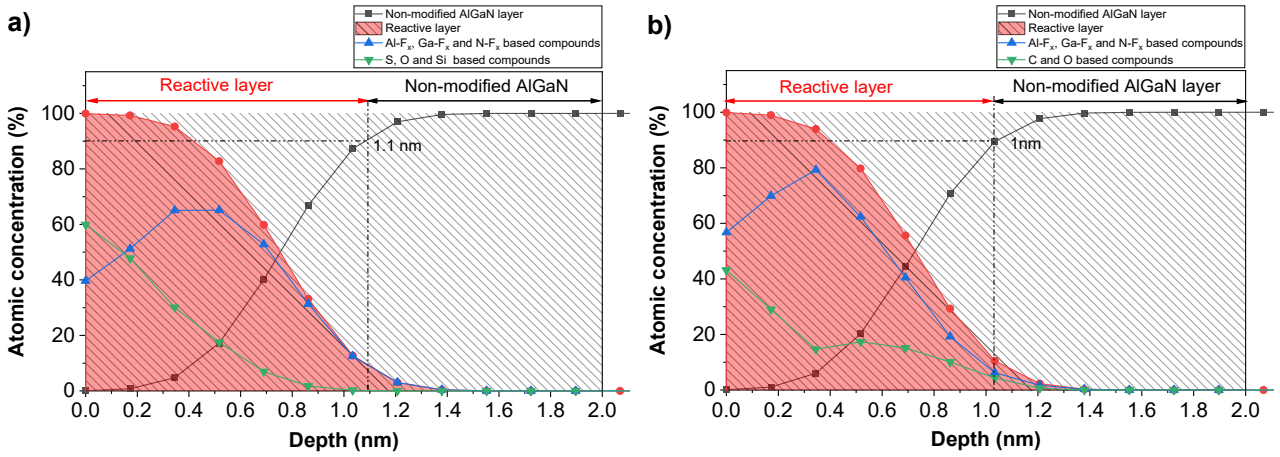

Fig. 10. Atomic concentration profiles measured by AR-XPS after SiN layer etching by (a) low-energy SF_6/Ar plasma, and (b) low-energy CHF_3/CF_4/Ar plasma.

The (Al+Ga)/N ratio evolution with the low-energy plasma process is shown in Fig.11. At low ion energy, there is also an N depletion, particularly pronounced with the SF_6/Ar plasma, but it is decreased compared to the respective high-energy processes. This indicates that the N depletion mechanism is a low-threshold ion energy reaction or a

spontaneous chemical reaction with atomic fluorine. A higher F^+/F flux in the low-energy SF_6/Ar plasma can explain the higher nitrogen depletion of the AlGaN. The increase of the ion energy leads to an increase in the nitrogen sputtering effect coupled with the activation of a chemical etching by fluorine which explains the higher nitrogen depletion in the high-energy process (cf. Fig.8).[28] Regarding the ratio Ga/Al, it remains similar to the reference AlGaN for both low-energy plasma processes. At low ion energy, there is no preferential etching of Ga compounds in the $CHF_3/CF_4/Ar$ plasma process. This suggests that there is an ion energy threshold for the sputtering of Ga-H_x compounds.

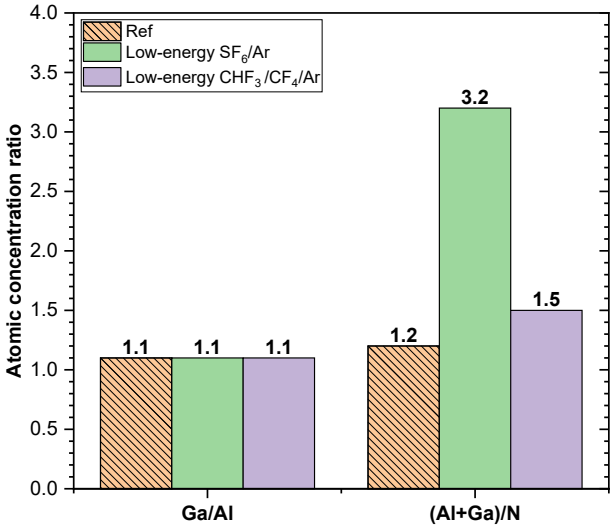

Fig. 11. The relative atomic concentration Al/Ga and (Al+Ga)/N ratios according to the plasma chemistry for low-energy SF_6/Ar and low-energy $CHF_3/CF_4/Ar$ plasma.

In addition, the E_F-E_{VBM} is determined for both low-energy plasma conditions (cf. Table V). The changes of the E_F-E_{VBM} at low-energy plasma are similar to the ones obtained at high-energy are 0.2 eV and 0.8 eV for $CHF_3/CF_4/Ar$ and SF_6/Ar, respectively. This indicates that ion energy does not seem to have a direct role in the Fermi level shift.

TABLE V. The E_F-E_{VBM} of the AlGaN surface after low-energy SF_6/Ar and low-energy CHF_3/CF_4/Ar plasma etching extracted from the valence-band spectrum measured by AR-XPS.

Samples	E_F-E_{VBM} (eV)
Reference	2.5
Low-energy SF_6/Ar	1.7
Low-energy CHF_3/ CF_4/Ar	2.3

To summarize, reducing the ion energy down to 15 eV in fluorine-based plasma processes leads to a reduction of SiN etch rate and suppression of AlGaN etching, leading to an infinite selectivity. A rich in fluorine $AlGaNF_x$, thick of about 1 nm is formed on the AlGaN surface. The initial reaction path for its formation is N removal, which leaves behind Ga and Al dangling bonds that will react with fluorine to form Al-F_x and Ga-F_x non-volatile compounds. The N removal can be attributed to several mechanisms occurring at the same time: Ar sputtering favored by increased ion energy, or chemical reaction with F^+/F to form volatile N-F_x.

Therefore, we can conclude that even if ion-driven processes are reduced by minimizing the ion energy, fluorine radicals can still induce some modification at the surface of the AlGaN that can eventually lead to degradation of the electrical performance.

C. Wet post-etching treatments

In order to clean and repair the AlGaN surface after etching, the next part of the article will focus on post-etching treatments. We focus on low ion energy processes that minimize the etch-induced damage. We used a post-etching treatment based on the KOH solution. This wet etching is typically used after dry etching to remove residues and clean the surface and restore plasma-induced damage.[33] The samples in Fig.1 (a) exposed to the two low-energy plasmas were then treated with wet KOH (40%) for 2 minutes, rinsed in

deionized water for 5 minutes, and then dried in a jet of N_2. After described post-etching treatment, the samples were analyzed by AR-XPS, TEM, and AFM analysis.

The Ga*3d* and Al*2p* core-level spectrum and surface composition measured by AR-XPS are presented in Fig.12 (a) and (b), respectively. The $AlGaNF_x$ modified layer is removed as confirmed by the disappearance of the fluorine-based peaks Ga-F_x (cf. Fig. 12.), and Al-F_x (cf. Fig.12 and Fig.13) and a significant decrease in the intensity of the F*1s* (cf. Fig.13) peak present at the AlGaN surface after etching.

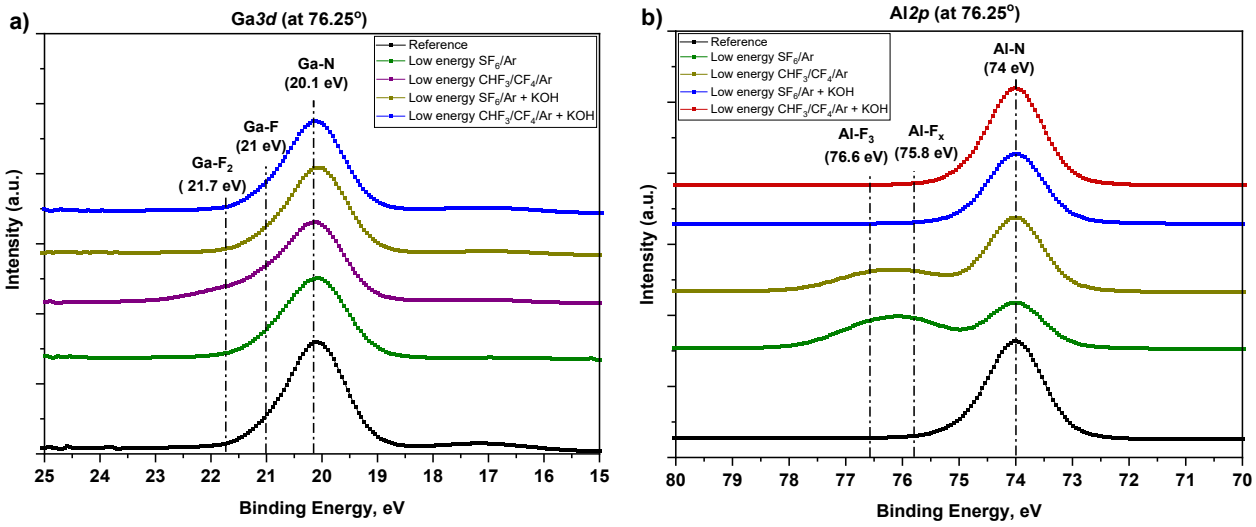

Fig. 12. (a) Ga*3d* and (b) Al*2p* core level deconvolution of AR-XPS measured spectra of the reference sample, the sample etched by low-energy SF_6/Ar and low-energy CHF_3/CF_4/Ar plasma, and the samples etched by low-energy SF_6/Ar and CHF_3/CF_4/Ar followed by KOH treatment.

Fig.13 shows the XPS analysis of the surface composition (at grazing angle 76.25°) of the samples etched by low-energy SF_6/Ar and CHF_3/CF_4/Ar plasma processes followed by KOH treatment. In both cases after KOH treatment, Al-F_x and Ga-F_x bonds are removed and less than 5% of F is detected on the surface, suggesting that the KOH treatment can

remove completely the $AlGaNF_x$ reactive layer formed after plasma exposure. In the case of low-energy SF_6/Ar plasma, the KOH treatment does not remove the Si contamination introduced by the plasma etching process.

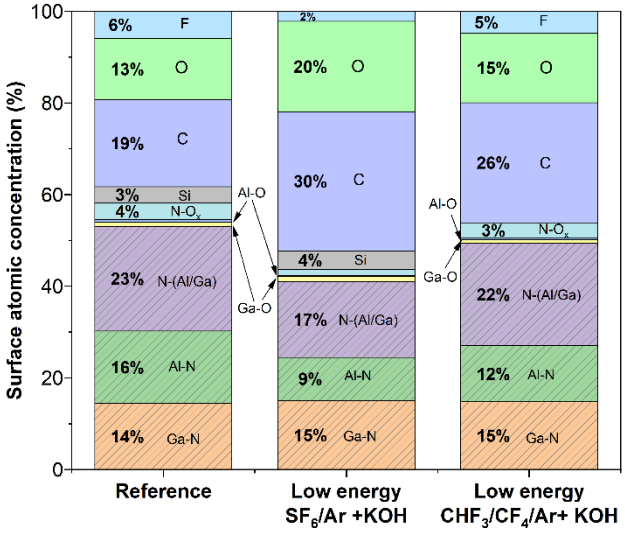

Fig. 13. The atomic composition of the AlGaN sample at grazing angle 76.25° (surface) for reference sample and samples after etching by low-energy SF_6/Ar and CHF_3/CF_4/Ar followed by KOH.

The AlGaN surface stoichiometry ratios for reference AlGaN sample and samples after etching by low-energy SF_6/Ar and CHF_3/CF_4/Ar followed by KOH are compared in Fig. 14.

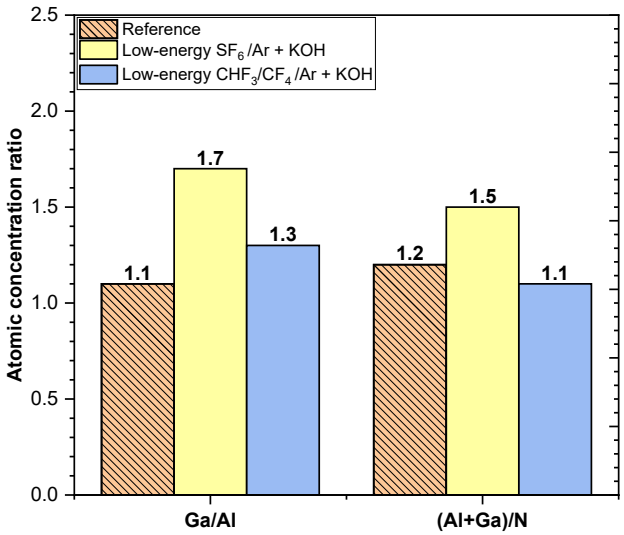

Fig. 14. The Ga/Al and (Al+Ga)/N ratios according to the plasma chemistry and post-treatment.

Even if no Al depletion was observed after plasma etching (cf. Fig.11), KOH treatment leads to Al depletion, especially with the low-energy SF_6/Ar plasma process. Indeed, in section III.B, it was observed that Al-N bonds are more likely transformed into Al-F_x bonds than Ga-N into Ga-F_x and that this effect is much more pronounced in the case of the SF_6/Ar plasma chemistry (cf. Fig.11). As the KOH treatment removes the fluorinated $AlGaNF_x$ reactive layer selectively over the non-modified AlGaN, and as Al is more fluorinated after plasma exposure, the AlGaN surface is depleted in Al after the KOH treatment, especially in the SF_6/Ar case. After KOH, the (Al+Ga)/N ratio is almost restored and similar to that of the reference sample, although the surface after low energy SF_6/Ar followed by KOH is still slightly depleted in N. This can be explained by the fact that the removal of N is deeper than the formation of Al-Fx and Ga-Fx bonds. As shown in Table VI, the removal of the $AlGaNF_x$ reactive layer after KOH post-treatment restores the E_F-E_{VBM} to the reference value in the case of low-energy SF_6/Ar but has no effect on the sample

etched with low-energy CHF_3/CF_4/Ar plasma for which the E_F-E_{VBM} remains 0.2 eV below the E_F-E_{VBM} of the reference.

TABLE VI. The E_F-E_{VBM} of the AlGaN surface after low-energy SF_6/Ar and low-energy CHF_3/CF_4/Ar plasma etching followed by KOH post-etching treatment extracted from the valence-band spectrum measured by AR-XPS.

Samples	**E_F-E_{VBM} (eV)**
Reference	2.5
Low-energy SF_6/Ar + KOH	2.5
Low-energy CHF_3/ CF_4/Ar KOH	2.3

Fig. 15 (a), (b), and (c) show the cross-section TEM images of the AlGaN/GaN films of the sample presented in Fig.1 (a) before SiN etching, and of the samples etched by low-energy SF_6/Ar and CHF_3/CF_4/Ar plasma followed by the KOH post-etching treatment. Before SiN etching, the AlGaN layer thickness is 5.8 nm. After low-energy SF_6/Ar and CHF_3/CF_4/Ar plasma etching followed by the KOH treatment, the AlGaN thickness is reduced to 5 nm and 4.8 nm, respectively. Therefore, the SiN cap etching leads to a 0.8 nm and 1 nm AlGaN recess when using low-energy SF_6/Ar and CHF_3/CF_4/Ar plasma processes respectively. This recess is due to the $AlGaNF_x$ reactive layer removal by KOH whose thickness has been estimated by AR-XPS of around 1 nm in both cases (cf. Fig.10 (a) and (b)). It is hard to conclude if the recess is more important in the case of low energy CHF_3/CF_4/Ar since the AlGaN thickness after epitaxy has a variability of ± 0.4 nm from the supplier specifications.

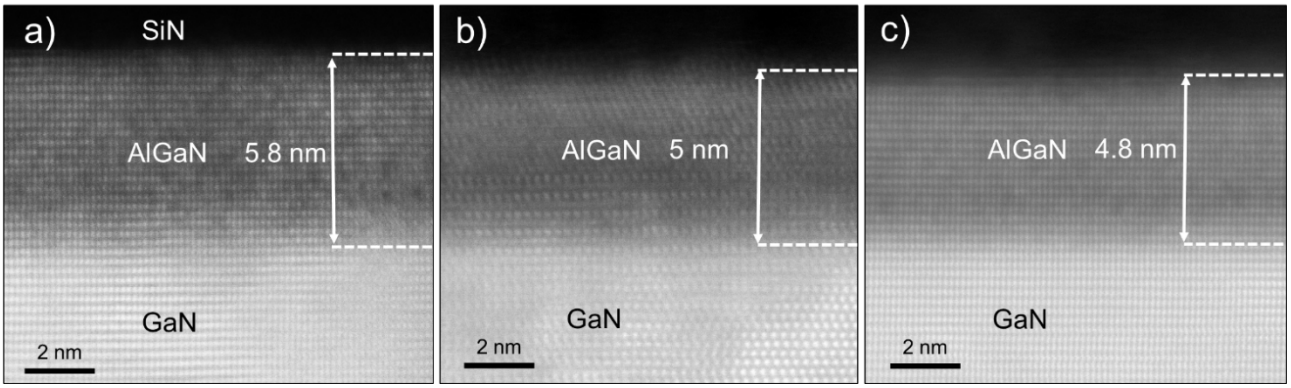

Fig. 15. Cross-section TEM image of the AlGaN/GaN layers for (a) Before SiN etching (b) sample after low-energy SF_6/Ar plasma etching followed by KOH treatment and (c) sample after low-energy CHF_3/CF_4/Ar plasma etching followed by KOH treatment.

Fig.16. shows AFM measurements performed on (a) reference sample (after BOE) and samples after low energy (b) SF_6/Ar and (c) CHF_3/CF_4/Ar plasma etching followed by KOH wet treatment. The reference sample after BOE etching shows clearly defined rounded atomic steps (cf. Fig.16). After low-energy SF_6/Ar and CHF_3/CF_4/Ar followed by KOH, the AlGaN surface morphology looks similar to the reference one. The Root Mean Square Roughness (RMS) and Maximum Roughness Depth (Rmax) values are slightly increased in both cases (RMS increased from 0.15 nm to 0.23 nm and 0.19 nm and Rmax increased from 1.5 nm to 2.7 nm and 1.9 nm for low-energy SF_6/Ar and CHF_3/CF_4/Ar plasmas followed by KOH, respectively). This augmentation is more accentuated in the case of low-energy SF_6/Ar. Atomic steps are still noticeable, but the blurred aspect of the image suggests a slight amorphization of the surface. Note that after the high ion energy process followed by KOH treatment, quite similar RMS roughness and surface morphology were observed (not shown here). This is somehow not surprising since the KOH step removes the $AlGaNF_x$ layer formed during the SiN plasma etching step.

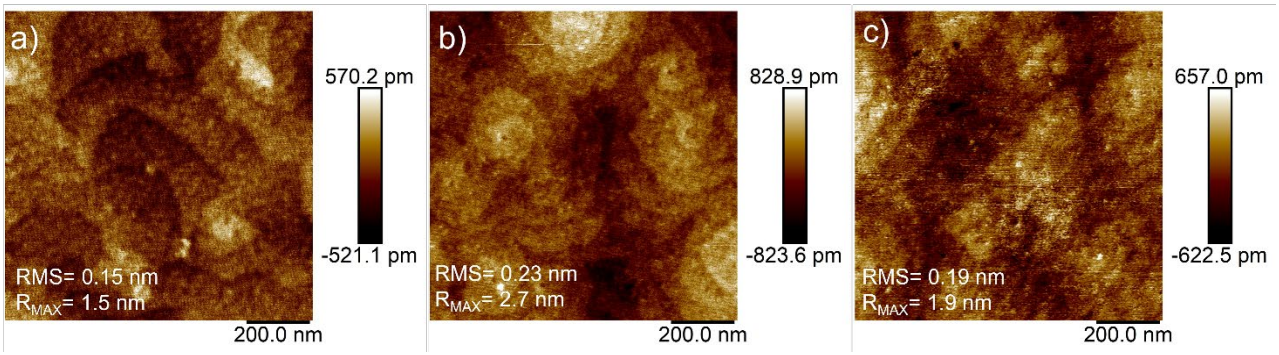

Fig. 16. AFM measurements of the AlGaN surface for (a) reference sample (after BOE) (b) sample after low-energy SF_6/Ar plasma etching followed by KOH treatment, and (c) sample after low-energy CHF_3/CF_4/Ar plasma etching followed by KOH treatment.

IV. CONCLUSIONS

The SiN cap layer etching with selective etching that stops on the AlGaN barrier layer is critical for the fabrication of MOS-HEMTs. In the present study, we have investigated the chemical and physical modifications induced to AlGaN layers exposed to high and low ion energy SF_6/Ar and CHF_3/CF_4/Ar plasma processes dedicated to the SiN etching. Changing the plasma chemistry from SF_6/Ar to CHF_3/CF_4/Ar improves the SiN/AlGaN selectivity. AR-XPS analyses performed on the AlGaN surface after both high energy plasma exposure indicate the important AlGaN surface modification by the formation of rich fluorine and N-depleted $AlGaNF_x$ layer. The depth of this modification is about 1.5 nm. The formation of this layer is supposed to start with N removal, which leaves Al and Ga dangling bonds that rapidly form non-volatile AlF_x and GaF_x products. The high ion energy SF_6/Ar plasma processes lead to a greater N depletion and Al-F_x/Ga-F_x ratio than the CHF_3/CF_4/Ar ones. However, while the high ion energy CHF_3/CF_4/Ar process presents a slight change of 0.2 eV in the Fermi level towards the valence band, the

high ion energy SF_6/Ar process leads to a 0.8 eV Fermi level shift towards the valence band.

In order to minimize the AlGaN surface modification, we developed the low ion energy SF_6/Ar and CHF_3/CF_4/Ar plasma processes. By decreasing the ion energy from 260 eV to 15 eV, infinite SiN/AlGaN etch selectivity can be obtained due to the formation $AlGaNF_x$ etch-stop layer on the AlGaN sub-surface. Both low-energy plasmas lead to a ~1 nm-thick modified layer whose thickness is driven by fluorine radicals diffusion. In the same way, as for the high-energy plasma process, the low ion energy CHF_3/CF_4/Ar process presents a slight change of 0.2 eV in the Fermi level towards the valence band, and the low ion energy SF_6/Ar process leads to a 0.8 eV Fermi level shift towards the valence band. This suggests that the Fermi level change is not correlated to the ion energy and is determined by plasma chemistry.

Furthermore, conventional post-treatment based on a wet KOH solution was used. After the KOH wet treatment, the $AlGaNF_x$ sub-surface reactive layer is completely removed in both low ion energy plasma processes. This removal leads to the recces (around 1 nm) of the AlGaN layer which is equivalent to the thickness of the $AlGaNF_x$ sub-surface reactive layer. After KOH treatment, the AlGaN stoichiometry is impacted by Al and N depletion in both low ion energy plasma cases. It can be explained by the fact that fluorine-based plasma leads to a greater Al fluorination over Ga and that KOH wet removes the Al-F_x and Ga-F_x compounds selectively over the Al-N and Ga-N bonds. In the case of the low ion energy SF_6/Ar process followed by KOH, the surface is more depleted in N. Although the AlGaN stoichiometry seems to be more degraded after low ion energy SF_6/Ar followed by KOH than after low ion energy CHF_3/CF_4/Ar followed by KOH, the Fermi level (E_F-

E_{VBM}), and the surface morphology are very close to the ones of the reference sample after BOE etching. These results indicate that the combination of a low ion energy plasma etching process, combined with a KOH wet post-treatment step leads to minimal surface modification and surface roughness, and is promising for high-performance MOS-HEMT devices fabrication.

ACKNOWLEDGMENTS

LN2 is a joint International Research Laboratory (IRL 3463) funded and co-operated by Université de Sherbrooke (Canada) and CNRS (France) as well as INSA Lyon, ECL, Université Grenoble Alpes (UGA). LN2 is supported by FRQNT.

This research was supported by the French RENATECH network and the Nano 2022 program.

AUTHOR DECLARATIONS

Conflict of Interest

The authors have no conflicts to disclose.

DATA AVAILABILITY

The data that support the findings of this study are available from the corresponding author upon reasonable request.

REFERENCES

[1] U.K. Mishra, P. Parikh, and Y.-F. Wu, Proc. IEEE **90**, 1022 (2002).
[2] F. Roccaforte, G. Greco, P. Fiorenza, and F. Iucolano, Materials **12**, 1599 (2019).
[3] M. Meneghini, C. De Santi, I. Abid, M. Buffolo, M. Cioni, R.A. Khadar, L. Nela, N. Zagni, A. Chini, F. Medjdoub, G. Meneghesso, G. Verzellesi, E. Zanoni, and E. Matioli, J. Appl. Phys. **130**, 181101 (2021).
[4] P.-C. Han, Z.-Z. Yan, C.-H. Wu, E.Y. Chang, and Y.-H. Ho, in *2019 31st Int. Symp. Power Semicond. Devices ICs ISPSD* (2019), pp. 427–430.
[5] S. Huang, X. Liu, X. Wang, X. Kang, J. Zhang, J. Fan, J. Shi, K. Wei, Y. Zheng, H. Gao, Q. Sun, M. Wang, B. Shen, and K.J. Chen, IEEE Trans. Electron Devices **65**, 207 (2018).
[6] T. Hashizume and H. Hasegawa, Appl. Surf. Sci. **234**, 387 (2004).
[7] B.D. Pant and U.S. Tandon, Plasma Chem. Plasma Process. **19**, 545 (1999).
[8] J.H. Ye and M.S. Zhou, J. Electrochem. Soc. **147**, 1168 (2000).
[9] D. Gahan, B. Dolinaj, and M.B. Hopkins, Rev. Sci. Instrum. **79**, 033502 (2008).
[10] N.S.J. Braithwaite, J.P. Booth, and G. Cunge, Plasma Sources Sci. Technol. **5**, 677 (1996).
[11] K. Takahashi, M.H.M. Hori, and T.G.T. Goto, Jpn. J. Appl. Phys. **33**, 4745 (1994).
[12] X.-J. Huang, Y. Xin, L. Yang, C. Ye, Q.-H. Yuan, and Z.-Y. Ning, Phys. Plasmas **16**, 043509 (2009).
[13]HORIBA JOBIN YVON; Data Analysis and Technical Report; Available online : https://www.horiba.com/int/scientific/technologies/spectroscopic-ellipsometry/data-analysis/
[14] L. Edwards, P. Mack, and D.J. Morgan, Surf. Interface Anal. **51**, 925 (2019).
[15] T. Meyer, C. Petit-Etienne, and E. Pargon, J. Vac. Sci. Technol. A **40**, 023202 (2022).
[16] C. Petit-Etienne, M. Darnon, L. Vallier, E. Pargon, G. Cunge, F. Boulard, O. Joubert, S. Banna, and T. Lill, J. Vac. Sci. Technol. B **28**, 926 (2010).
[17] J.H. Scofield, J. Electron Spectrosc. Relat. Phenom. **8**, 129 (1976).
[18] O. Joubert, G. Cunge, B. Pelissier, L. Vallier, M. Kogelschatz, and E. Pargon, J. Vac. Sci. Technol. Vac. Surf. Films **22**, 553 (2004).
[19] T. Hashizume, S. Ootomo, S. Oyama, M. Konishi, and H. Hasegawa, J. Vac. Sci. Technol. B Microelectron. Nanometer Struct. Process. Meas. Phenom. **19**, 1675 (2001).
[20] R. Sohal, P. Dudek, and O. Hilt, Appl. Surf. Sci. **256**, 2210 (2010).
[21] S. Huang, H. Chen, and K.J. Chen, Phys. Status Solidi C **8**, 2200 (2011).
[22] P. Alnot, J. Olivier, F. Wyczisk, and R. Joubard, J. Electrochem. Soc. **136**, 2361 (1989).
[23] K.L. Seaward, N.J. Moll, and W.F. Stickle, J. Electron. Mater. **19**, 385 (1990).
[24] M.L. Yu, K.Y. Ahn, and R.V. Joshi, J. Appl. Phys. **67**, 1055 (1990).
[25] C. Cardinaud, A. Rhounna, G. Turban, and B. Grolleau, J. Electrochem. Soc. **135**, 1472 (1988).
[26] G.H. Kim, W.H. Jeong, and H.J. Kim, Phys. Status Solidi A **207**, 1677 (2010).
[27] W.M. Haynes, *CRC Handbook of Chemistry and Physics* (CRC Press, 2014).
[28] C. Steinbrüchel, Appl. Phys. Lett. **55**, 1960 (1989).
[29] M. Higashiwaki, S. Chowdhury, B.L. Swenson, and U.K. Mishra, Appl. Phys. Lett. **97**, 222104 (2010).

[30] O. Ambacher, J. Smart, J.R. Shealy, N.G. Weimann, K. Chu, M. Murphy, W.J. Schaff, L.F. Eastman, R. Dimitrov, L. Wittmer, M. Stutzmann, W. Rieger, and J. Hilsenbeck, J. Appl. Phys. **85**, 3222 (1999).
[31] P. Brichon, E. Despiau-Pujo, and O. Joubert, J. Vac. Sci. Technol. A **32**, 021301 (2014).
[32] J.F. Ziegler and J.P. Biersack, in *Treatise Heavy-Ion Sci. Vol. 6 Astrophys. Chem. Condens. Matter*, edited by D.A. Bromley (Springer US, Boston, MA, 1985), pp. 93–129.
[33] L.-C. Chang, T.-H. Tsai, Y.-H. Jiang, and C.-H. Wu, in *2016 IEEE Int. Conf. Electron Devices Solid-State Circuits EDSSC* (2016), pp. 422–425.